

SUPPORTING INFORMATION FOR

Selenomethionine Quenching of Tryptophan Fluorescence Provides a Simple Probe of Protein

Structure

Matthew D. Watson[†], Ivan Perant[†], Junjie Zou, Osman Bilsel and Daniel P. Raleigh*

[†]These authors contributed equally to this work

*Person to whom correspondence should be addressed

Estimation of Helical Content

The percent of helical structure in the 21 residue helical peptide was calculated from the molar ellipticity at 222 nm, $[\theta]_{obs}$ using the the expression

$$f_h = \frac{[\theta]_{obs} - [\theta]_c}{[\theta]_H - [\theta]_c} \quad (S1)$$

Where $[\theta]_H$ is the molar ellipticity at 222 nm for a 100% helical peptide and $[\theta]_c$ is the molar ellipticity at 222 nm for a random coil:

$$[\theta]_H = -40000 \left(1 - \frac{2.5}{n} \right) + 100T \quad (S2)$$

$$[\theta]_c = 640 - 45T \quad (S3)$$

Where n is the number of residues in the peptide and T is the temperature in °C.¹

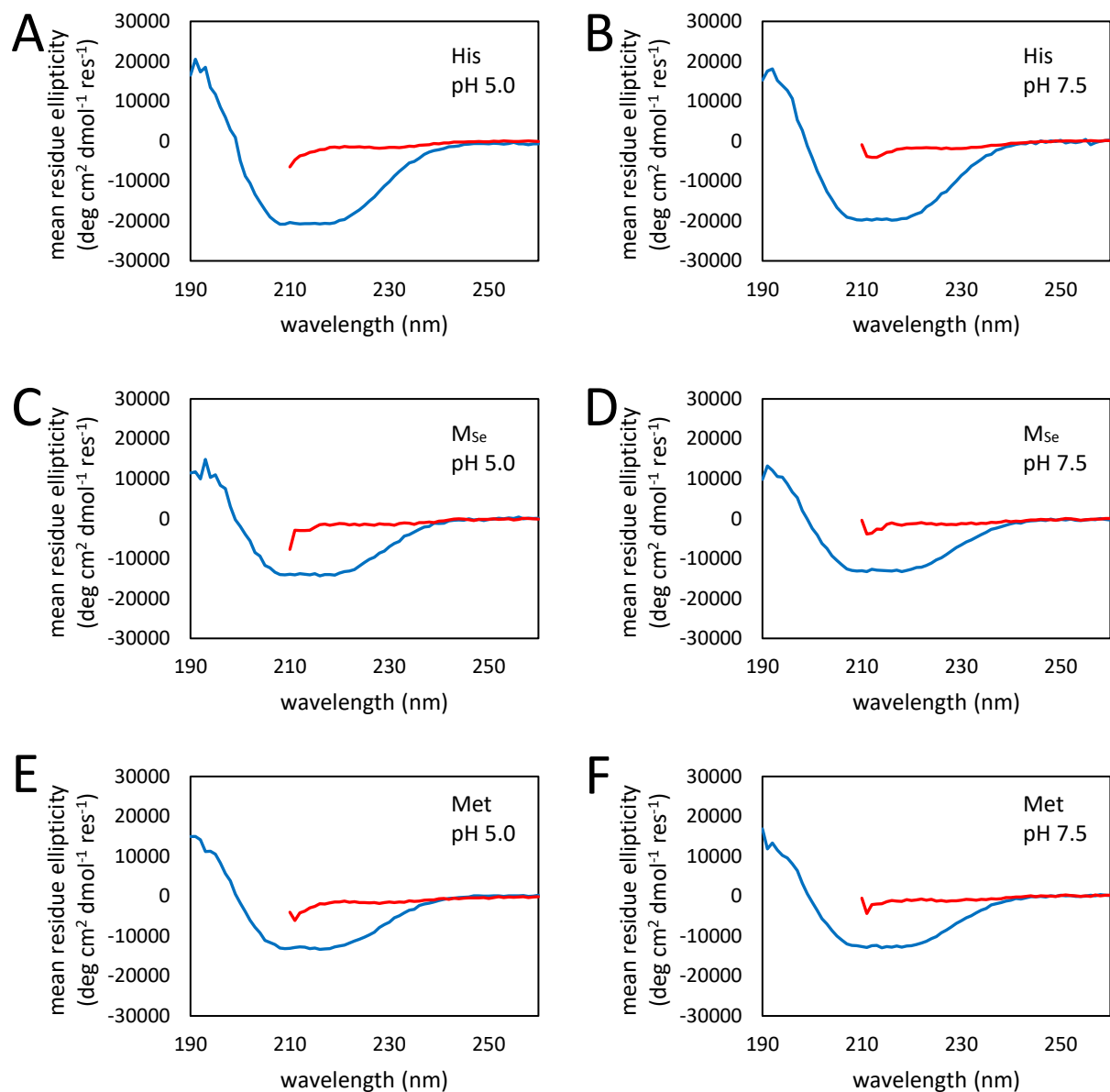


Figure S1: (A) CD spectra of Y126W-CTL9 at 20 °C in 20 mM acetate buffer at pH 5.0 (blue) and in the same buffer with 9.5 M urea (red). (B) CD spectra of Y126W-CTL9 at 20 °C in 20 mM tris buffer at pH 7.5 (blue) and in the same buffer with 9.5 M urea (red). (C) CD spectra of Y126W/H144M_{Se}-CTL9 at 20 °C in 20 mM acetate buffer at pH 5.0 (blue) and in the same buffer with 9.5 M urea (red). (D) CD spectra of Y126W/H144M_{Se}-CTL9 at 20 °C in 20 mM tris buffer at pH 7.5 (blue) and in the same buffer with 9.5 M urea (red). (E) CD spectra of Y126W/H144M-CTL9 at 20 °C in 20 mM acetate buffer at pH 5.0 (blue) and in the same buffer with 9.5 M urea (red). (F) CD spectra of Y126W/H144M-CTL9 at 20 °C in 20 mM tris buffer at pH 7.5 (blue) and in the same buffer with 9.5 M urea (red). The protein concentration in all samples was 25 μM.

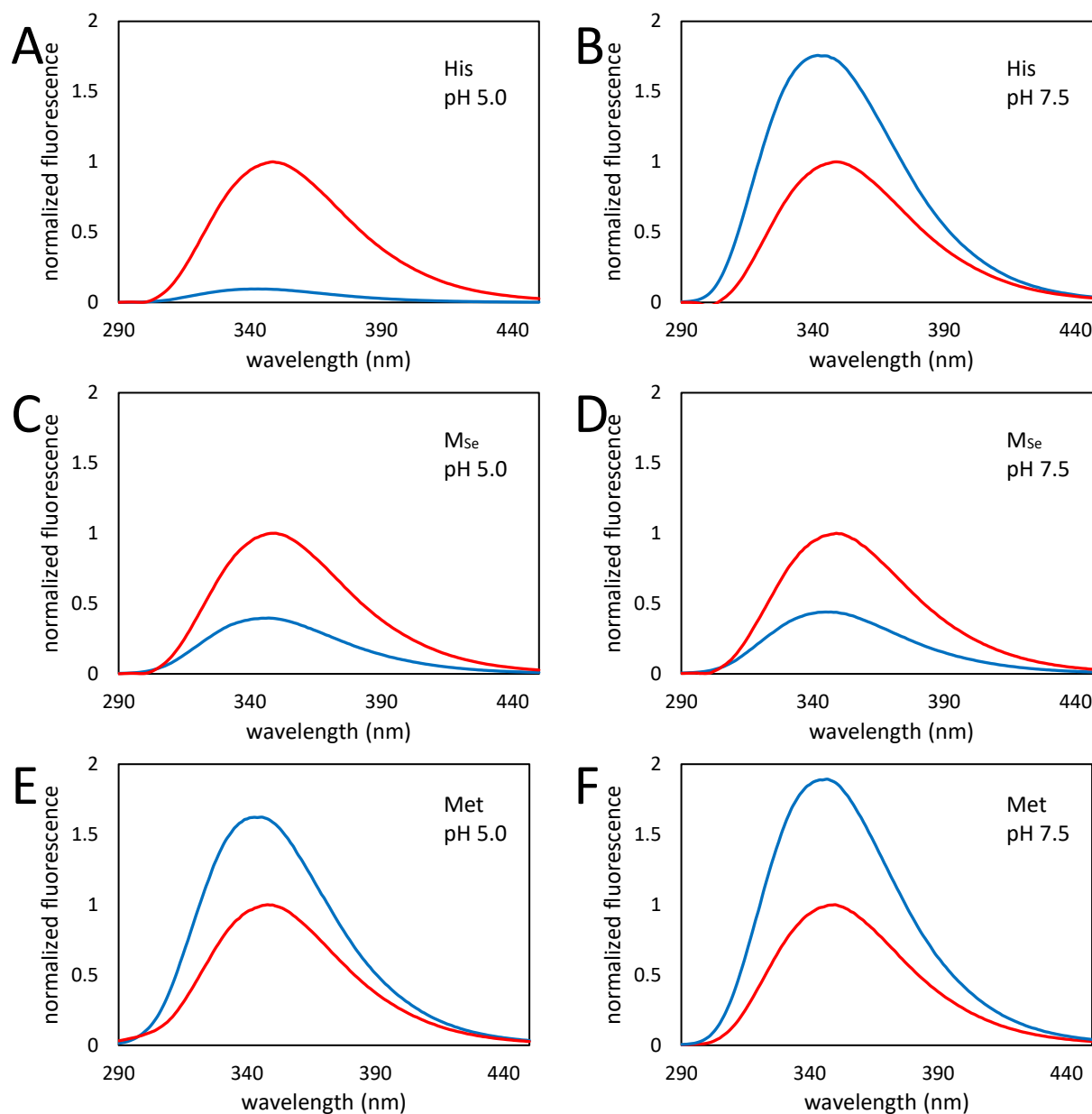


Figure S2: (A) Fluorescence emission spectra of Y126W-CTL9 at 20 °C in 20 mM acetate buffer at pH 5.0 (blue) and in the same buffer with 9.5 M urea (red). (B) Fluorescence emission spectra of Y126W-CTL9 at 20 °C in 20 mM tris buffer at pH 7.5 (blue) and in the same buffer with 9.5 M urea (red). (C) Fluorescence emission spectra of Y126W/H144M_{Se}-CTL9 at 20 °C in 20 mM acetate buffer at pH 5.0 (blue) and in the same buffer with 9.5 M urea (red). (D) Fluorescence emission spectra of Y126W/H144M_{Se}-CTL9 at 20 °C in 20 mM tris buffer at pH 7.5 (blue) and in the same buffer with 9.5 M urea (red). (E) Fluorescence emission spectra of Y126W/H144M-CTL9 at 20 °C in 20 mM acetate buffer at pH 5.0 (blue) and in the same buffer with 9.5 M urea (red). (F) Fluorescence emission spectra of Y126W/H144M-CTL9 at 20 °C in 20 mM tris buffer at pH 7.5 (blue) and in the same buffer with 9.5 M urea (red). Note that panels (B), (D) and (F) are included in Figure 1 of the manuscript and are reproduced here for clarity. The protein concentration in all samples was 25 μ M.

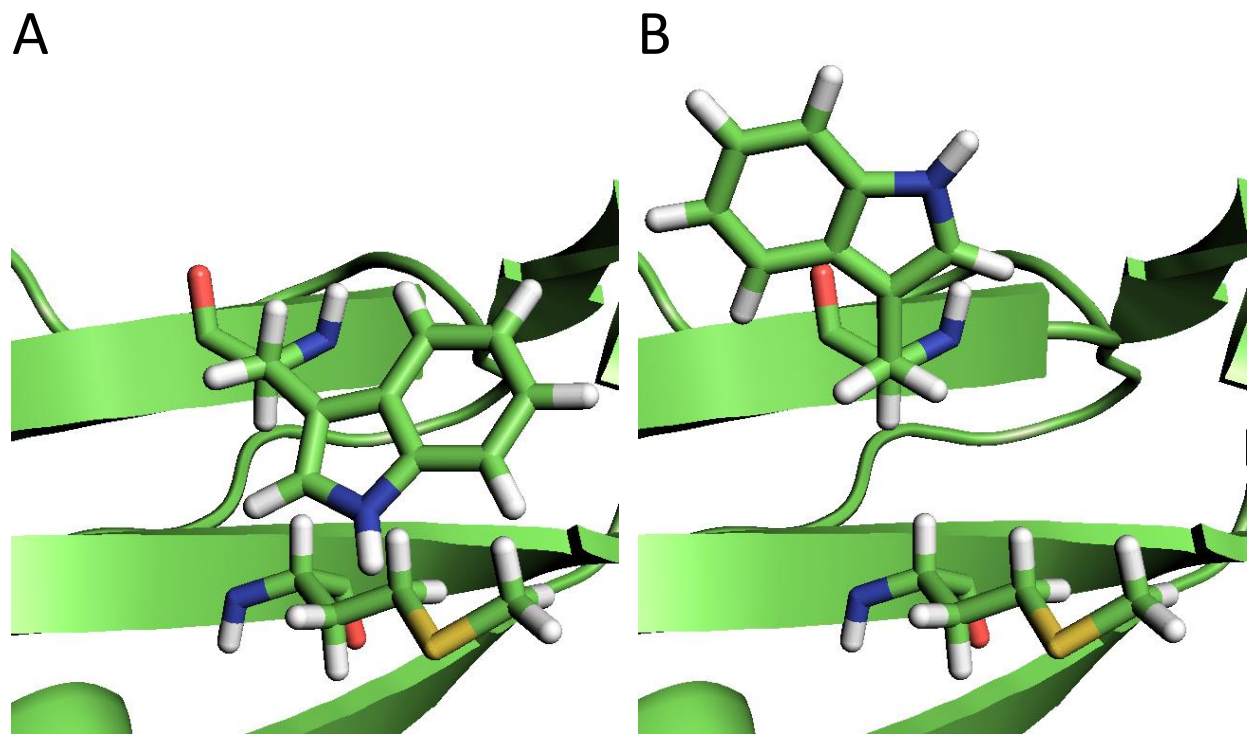


Figure S3: Models of the allowed χ_1 rotamers for Y126W/H144M_{se}-CTL9 based on PDB structure 1DIV.² **(A)** The $\chi_1 \approx -60^\circ$ rotamer, which corresponds to the orientation of the phenol ring of Tyr in the crystal structure, packing the indole ring against the M_{se} sidechain. **(B)** The $\chi_1 \approx 60^\circ$ rotamer, which exposes the Trp sidechain to solvent and moves the indole ring out of van der Waals contact with the Se atom.

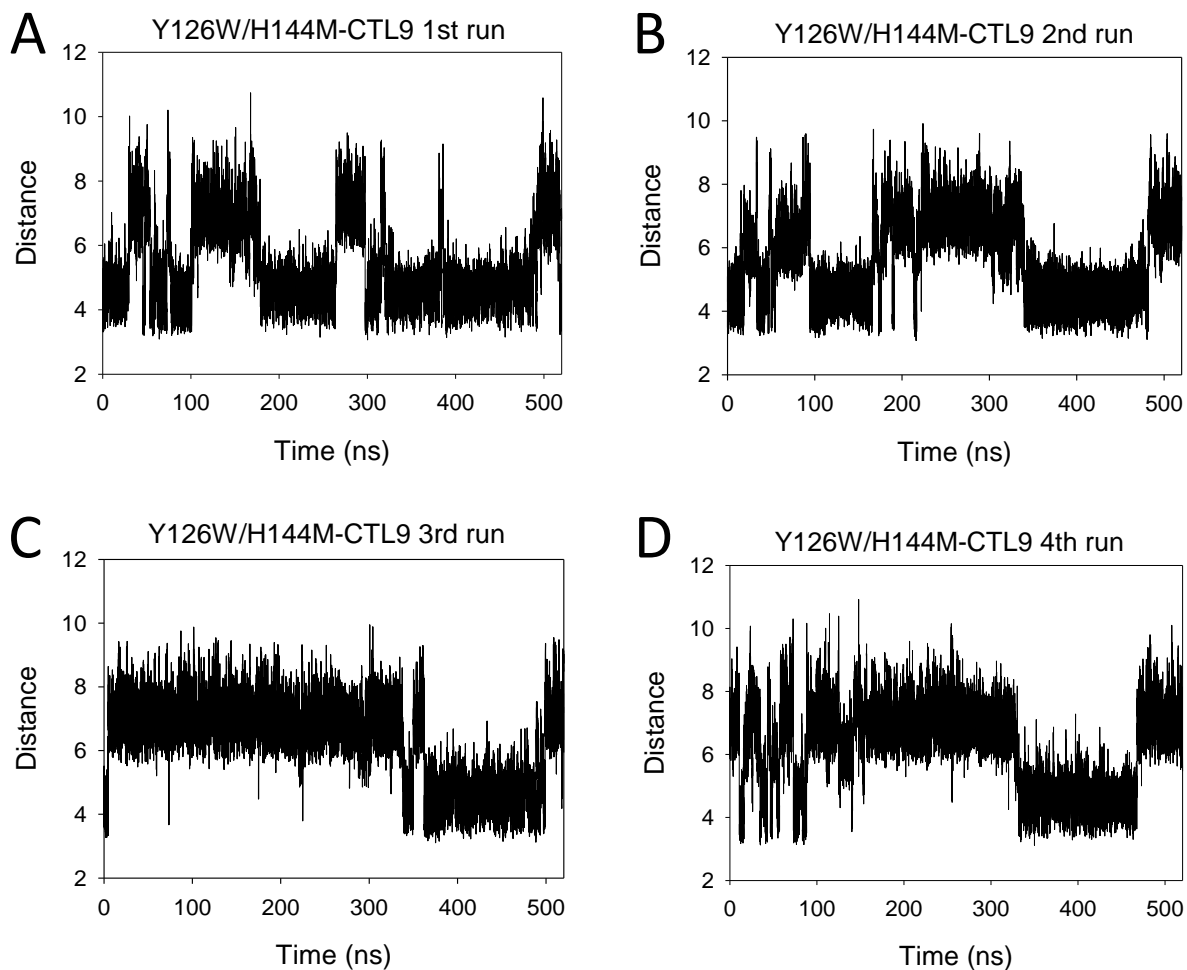


Figure S4. Distance in Å between the geometric center of C δ 2 and C ϵ 2 of the Trp indole ring and sulfur atom of Met during the MD simulations of Y126W/H144M-CTL9. **(A)** and **(B)** Independent MD simulations in which W126 starts with the rotamer $\chi_1 = -65.0^\circ$, $\chi_2 = -84.9^\circ$ **(C)** MD simulation in which W126 starts with the rotamer $\chi_1 = -71.2^\circ$, $\chi_2 = 94.3^\circ$ **(D)** MD simulation in which W126 starts with the rotamer $\chi_1 = 62.1^\circ$, $\chi_2 = 94.4^\circ$

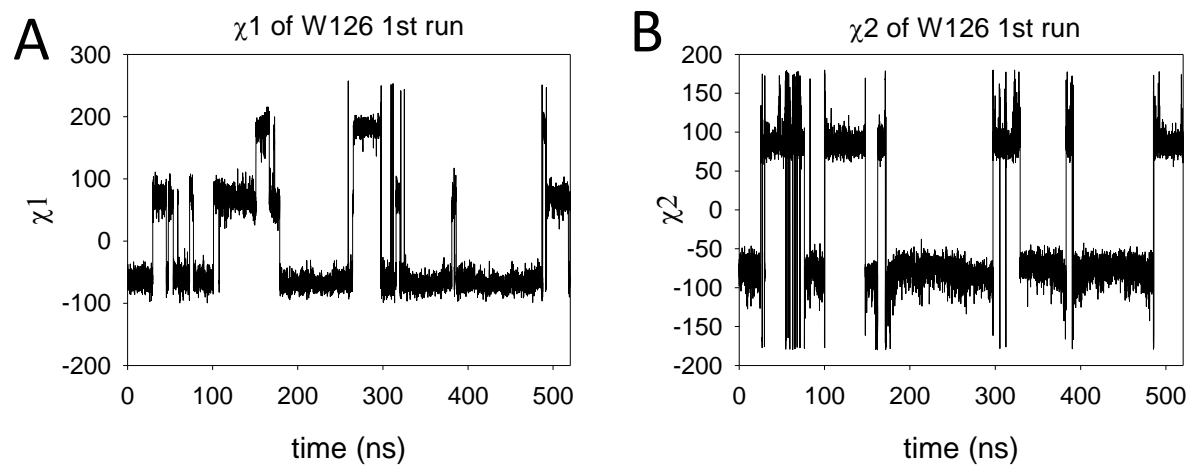


Figure S5. The χ_1 and χ_2 dihedral angles of W126 in Y126W/H144M-CTL9 during the 1st run of the MD simulations in which W126 starts with a rotamer state of $\chi_1 = -65.0^\circ$, $\chi_2 = -84.9^\circ$ **(A)** The χ_1 angle of W126 in degrees vs time. **(B)** The χ_2 angle of W126 in degrees vs time.

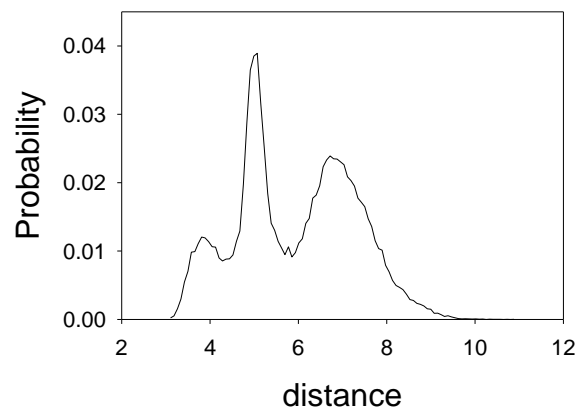


Figure S6. A histogram showing the distribution of the distances between W126 and M144 in Y126W/H144M-CTL9 collected from all 4 MD simulations. The distance was measured between the geometric center of C δ 2 and C ϵ 2 of the Trp indole ring and the sulfur atom of Met.

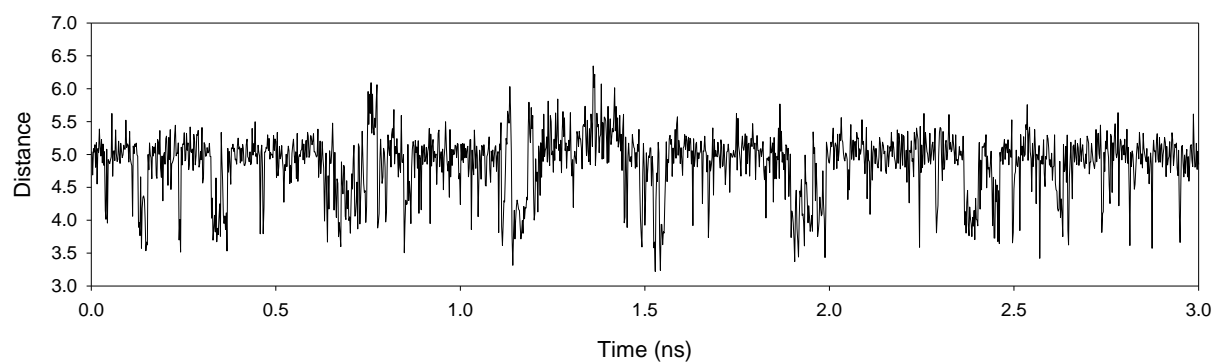


Figure S7. The distance between W126 and M144 of Y126W/H144M-CTL9 during a 3 ns MD simulation with a sampling frequency of 0.002 ns.

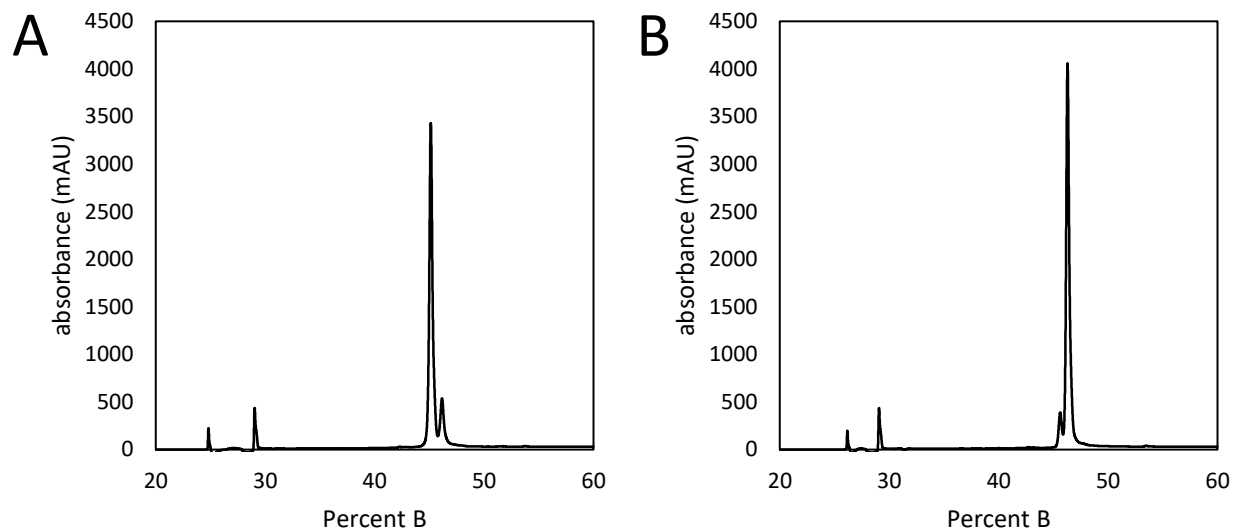


Figure S8. Selenomethionine is efficiently oxidized by 0.005% H_2O_2 while methionine is not. **(A)** Preparative HPLC trace of Y126W/H144M_{Se}-CTL9 after oxidation in 0.005% H_2O_2 for 4 hr. The peak centered at 45% B was identified by LC-ESI-TOF MS as Y126W/H144M_{SeO}-CTL9 and the peak centered at 46% B was identified as Y126W/H144M_{Se}-CTL9. **(B)** Preparative HPLC trace of Y126W/H144M-CTL9 after oxidation in 0.005% H_2O_2 for 4 hr. The peak centered at 46% B was identified by LC-ESI-TOF MS as Y126W/H144M_{ox}-CTL9 and the peak centered at 47% B was identified as Y126W/H144M-CTL9. The absorbance was monitored at 220 nm.

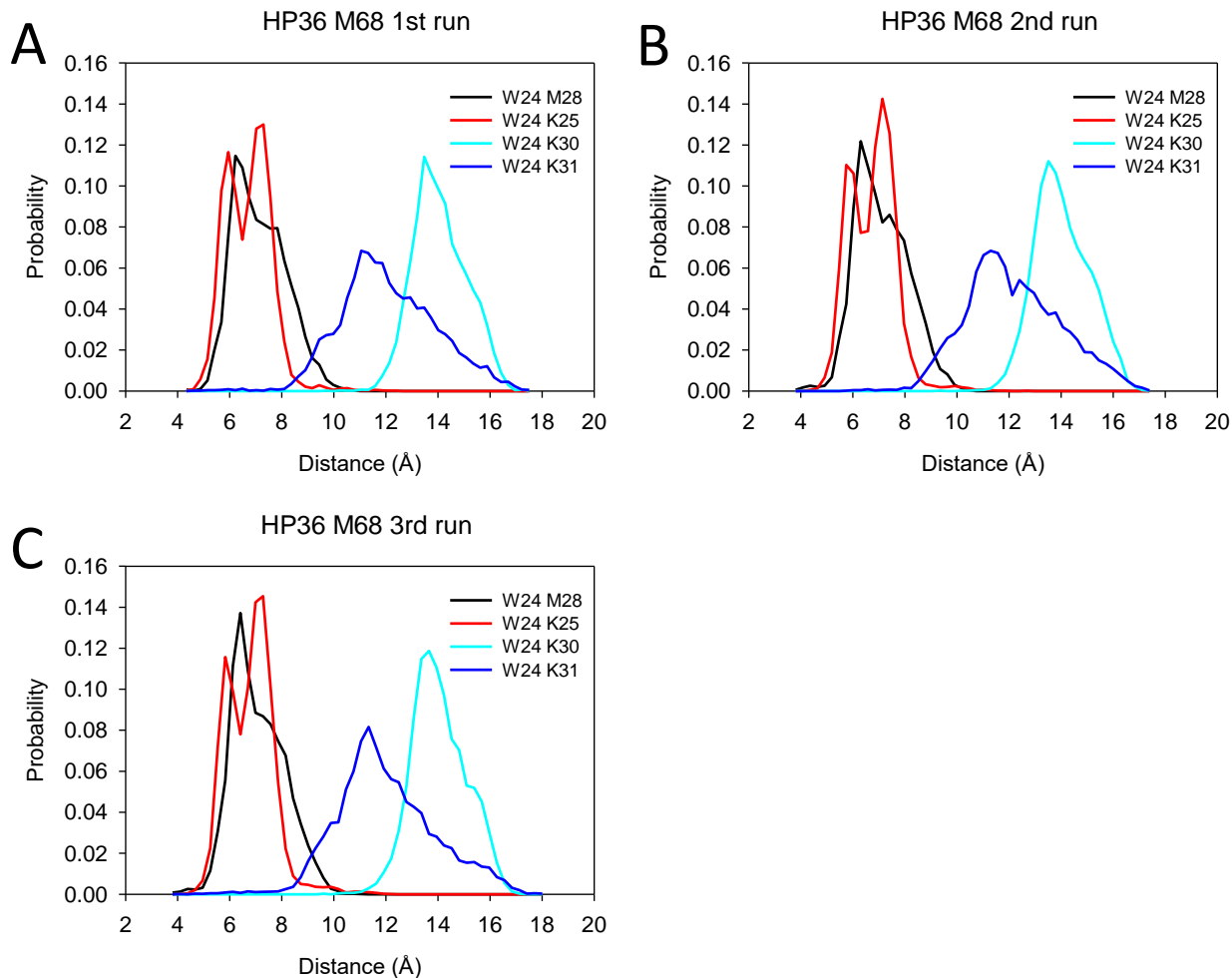


Figure S9. Distribution of distances between W24/M28, W24/K25, W24/K30 and W24/K31 in N28M-HP36 from the last 300 ns of three independent 400 ns MD simulations, which used starting structures with different rotamer states of W24. **(A)** $\chi_1 = 63.2^\circ$, $\chi_2 = 85.5^\circ$ **(B)** $\chi_1 = -82.2^\circ$, $\chi_2 = -89.3^\circ$ **(C)** $\chi_1 = -177.0^\circ$, $\chi_2 = 75.0^\circ$

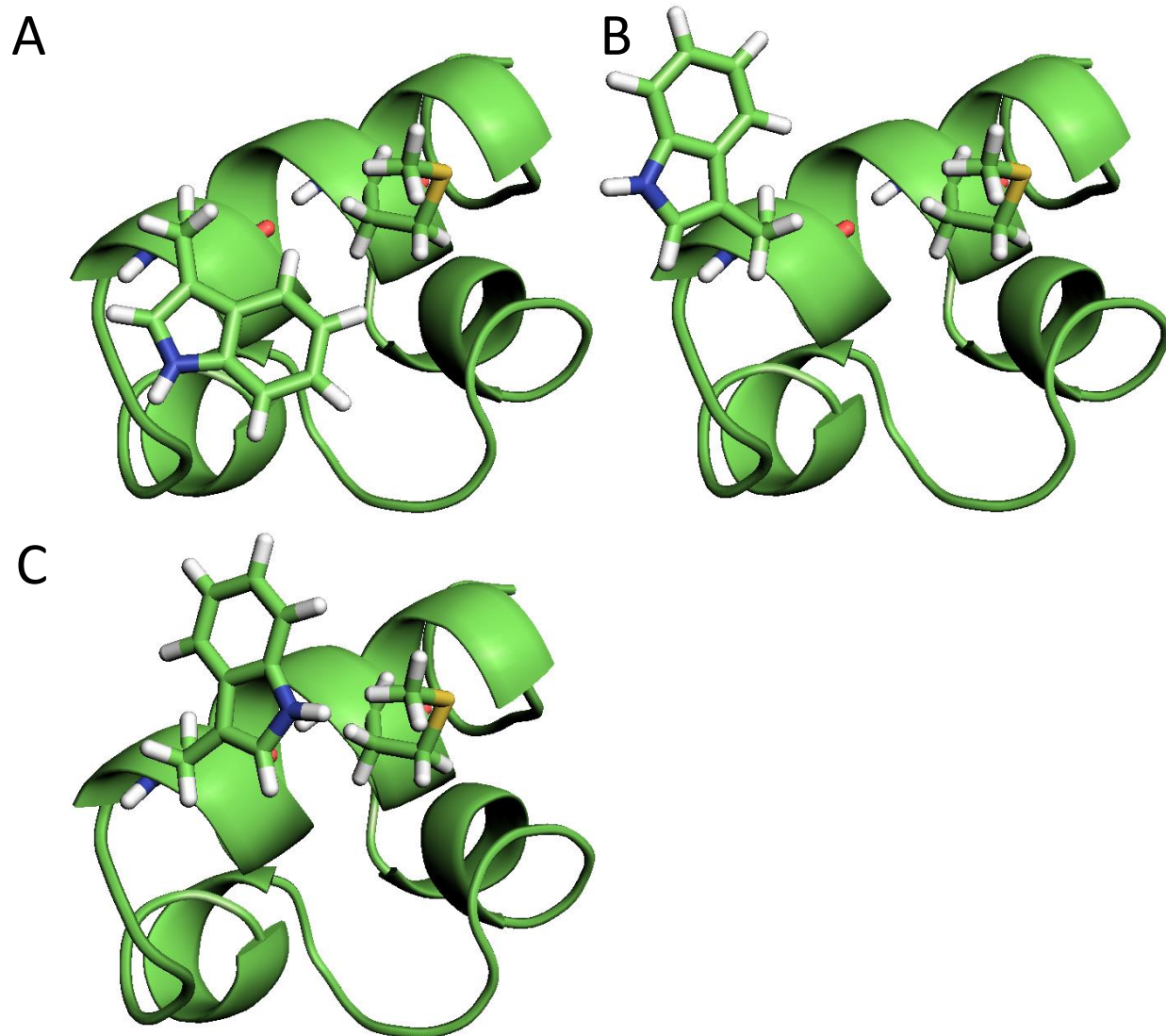


Figure S10: Models of the allowed χ_1 rotamers for N28M_{Se}-HP36 based on PDB structure 1VII.³ **(A)** The $\chi_1 \approx 60^\circ$ rotamer, the orientation from the crystal structure, which may bring the indole ring into transient contact with the Se atom. **(B)** The $\chi_1 \approx -60^\circ$ rotamer, which exposes the Trp sidechain to solvent and moves the indole ring out of van der Waals contact with the Se atom. **(C)** The $\chi_1 \approx 180^\circ$ rotamer, which brings the indole ring into close contact with the Se atom.

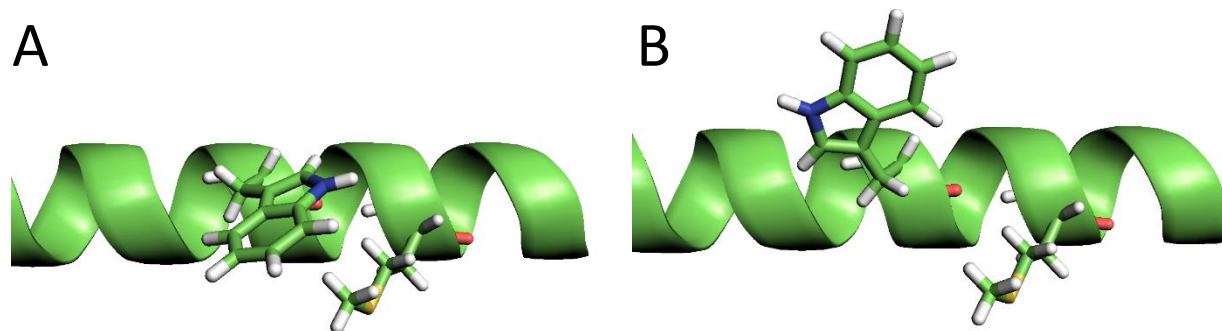


Figure S11: Models of the allowed χ_1 rotamers for the 21 residue helical peptide. **(A)** The $\chi_1 \approx 180^\circ$ rotamer, which brings the indole ring into close contact with the Se atom. **(B)** The $\chi_1 \approx -60^\circ$ rotamer, which moves the indole ring out of van der Waals contact with the Se atom.

Supporting References

- [1] Kuhlman, B., Yang, H. Y., Boice, J. A., Fairman, R., and Raleigh, D. P. (1997) An exceptionally stable helix from the ribosomal protein L9: implications for protein folding and stability, *J Mol Biol* 270, 640-647.
- [2] Hoffman, D. W., Davies, C., Gerchman, S. E., Kycia, J. H., Porter, S. J., White, S. W., and Ramakrishnan, V. (1994) Crystal structure of prokaryotic ribosomal protein L9: a bi-lobed RNA-binding protein, *EMBO J* 13, 205-212.
- [3] McKnight, C. J., Matsudaira, P. T., and Kim, P. S. (1997) NMR structure of the 35-residue villin headpiece subdomain, *Nat Struct Biol* 4, 180-184.